RESEARCH

VNIR–SWIR reflectance spectroscopy as a nondestructive technique for compositional determination of archaeological talc samples with a machine learning approach

M. Ferrer-Julià[1] · A. Quirós[1] · D. Herrero-Alonso[2] · E. González[1] · E. García-Meléndez[1]

Abstract

The material from which an archaeological piece is made provides a great deal of information regarding the society in which it was made; thus, any misidentification can lead to erroneous conclusions. The uniqueness of many of these pieces hinders their mineralogical analysis because the pieces cannot be damaged for sampling; therefore, errors in the classification of these materials are common. In the present study, we evaluate the suitability of the spectroradiometry technique in the analysis of two archaeological talc pieces. Both came from the Iron Age archaeological site of Peña del Castro (La Ercina, León) in the northwestern Iberian Peninsula. We compared the spectral curves of these 2 pieces with the spectral curves from 50 talc geological samples from different geographical sources, combining bulk and powdered samples. Our results show that spectral curves enabled the identification of the talc material in the powdered and bulk samples. Moreover, the absence of the talc characteristic features in other soft materials also used in antiquity enabled the detection of incorrect identification of the classified pieces. Even though our results cannot be used to define any absorption feature characteristic to establish the provenance of the material, in the present study, spectral analysis has been shown to be suitable as a nondestructive technique to mineralogically identify archaeological pieces.

Keywords Classification algorithms · Iberian Peninsula · Iron Age · Mineralogy · Spectroscopy

Introduction

The presence of easily shaped rocks, such as talc, is frequently observed in the archaeological record, in particular among food-producing groups from the Neolithic period onwards. Talc has been employed in the crafting of decorative pieces or for specific purposes, such as figurines or necklace beads. One of the reasons for the widespread use of this material is its appearance and color: talc exhibits a broad spectrum of colors, including green, white, pink, and black pieces, depending on its purity (Pi-Puig et al. 2020), which makes it highly appealing for ornamental purposes. Another contributing factor is its softness, facilitating easy manipulation and shaping.

In the Iberian Peninsula, talc has been used for different purposes, including the manufacturing of casting molds (Lackinger 2014), as an element of ornamentation through beads and pendants (Villalobos García 2016), and as inclusions in ceramic decorations (Lantes-Suárez et al. 2009). Items such as spindle whorls are prevalent in Iron Age sites in the north-western part of the Iberian Peninsula (Luengo 1940; Celis Sánchez 2007; Celis Sánchez and Grau Lobo 2007; Romero Carnicero and Górriz Gañán 2007; Marín Suárez 2011; Escortell and Maya 1972).

These whorl pieces are black, composed of talc, and, in some instances, contain pyrites. This mineral is found in the La Respina Mine, situated in the municipality of Puebla de Lillo, León (Galán-Huertos and Rodas 1973), just a few kilometers from the Peña del Castro site. This proximity suggests that the mine might be the source of the material used in the spindle whorls discovered. However, in the northern half of the

✉ A. Quirós
alicia.quiros@unileon.es

[1] Research Group On Environmental Geology, Biological and Environmental Sciences Faculty, Quaternary and Geodiversity (Q-GEO), Universidad de León, Campus de Vegazana, s/n, 24071 León, Spain

[2] Research Group On Estudos de Arqueoloxía, Antigüidade E Territorio (GEAAT), Departamento de Historia, Arte E Xeografía, Facultade de Historia, Universidade de Vigo, Campus Universitario As Lagoas, 32004 Ourense, Spain

Iberian Peninsula, other outcrops of talc and steatite are also present. These minerals are similar, making it challenging to differentiate them at the macroscopic level (Lackinger 2014). Therefore, the possibilities of sourcing this material could be much greater. Nevertheless, the identification of these pieces has been exclusively visual, lacking a mineralogical analysis to confirm their composition and potential provenance.

The mineralogical study of archaeological pieces presents several challenges, as discussed in the present work. First, samples cannot be destroyed or pulverized. Many of these artifacts are unique and decorated, making it imperative to analyze them through nondestructive techniques. As explained below, this poses a challenge when comparing them with geological reference samples that have been pulverized, regarding the potential equivalence between measurements of bulk and powdered samples. Moreover, many of these artifacts are deposited in museums; extracting them from these institutions is a complicated task as this poses a risk to their conservation. Therefore, the technique used for their analysis must be portable. Lastly, their study must be conducted quickly and economically. Vis-NIR-SWIR spectroradiometry meets all these requirements, as hyperspectral image analysis represents a noninvasive method for in situ analyses of stone surfaces (Picollo et al. 2020; Vettori et al. 2008).

La Peña del Castro site

La Peña del Castro site presents the largest number of talc pieces; furthermore, the entire operational chain of talc piece production has been found in this settlement, ranging from raw material blocks to preforms and finished objects. Considering that operational chains are not often found complete, we chose La Peña del Castro as the archaeological site in which to conduct the analyses proposed in the present work.

La Peña del Castro is situated in the northern part of the Iberian Peninsula (Spain), specifically in La Ercina town (province of León). Situated on a limestone platform in the transitional zone between the High Mountains of the Cantabrian Range and the León Highlands, the site controls the crossing zones between these two geomorphological units and is part of a network of similar settlements distributed along the fault that runs from east to west along the southern edge of the Cantabrian Mountains (Gutiérrez González 1986–87). This archaeological site reflects a prolonged occupation spanning from the end of the I Iron Age to the early stages of the Roman Empire. However, the peak expansion of the settlement occurred at the end of the II Iron Age.

The occupation of the site developed on the northern and western slopes, modifying and adapting the natural slope of the hill for the construction of the hamlet on three platforms limited by stone walls (González Gómez de Agüero et al. 2015, 2018), divided into four enclosures (Supplementary Fig. S1). A comprehensive occupational sequence with

four distinct phases was established through archaeological interventions conducted between 2013 and 2019. The talc pieces studied in the present work belong to the third phase of occupation, spanning the II–I centuries BC and coinciding with the settlement's maximum extension, covering the entire hill. The building structures of this phase exhibit a predominantly oval shape with stone plinths and mud-and-wood elevations (Es-05, Es-3/2, Es-8/1). Test Pit 01 revealed a rectangular dwelling composed of multiple rooms, resembling those documented in the plateau area (Es-06). Adjacent to the dwellings, a warehouse (Es-07) and two communal stone structures (Es-04 and Es-09) were identified (González Gómez de Agüero et al. 2023).

Around the change of Era, coinciding with the incorporation of the area into Roman administration, a violent destruction of the settlement occurred, marked by a significant fire that consumed the structures and sealed the occupation levels (González Gómez de Agüero et al. 2015, 2018).

Objectives

Our first objective is the mineralogical identification of the archaeological pieces from La Peña del Castro. Given that talc is not the only easily shaped and colorful mineral, pieces in archaeological collections are often misidentified from a mineralogical perspective. This misclassification and misinterpretation of 'talc' pieces can hinder our understanding of their historical significance.

The second objective is to validate Vis-NIR-SWIR spectroradiometry as a nondestructive and portable technique for mineralogical analysis. Recently, various spectroscopic techniques have been applied to investigate the mineral composition of archaeological artifacts. While most publications focus on the identification of flint pieces (Hubbard et al. 2004; Parish 2011, 2013, 2016, 2018; Rincón Ramírez 2012; Parish and Werra 2018; García del Moral et al. 2021), ceramics (Fischer and Hsieh 2017; Bruni 2022), and various elements of art and the conservation of cultural property (Wisseman et al. 2004; Liang 2012; Cheilakou et al. 2014; Siozos et al. 2017), the application of these techniques has recently become more common and can extend to other materials. Although the present study is not a representation of the state of the art in this field, its relevance lies in applying this technique to talc in particular, which is rare in previous literature..

The third objective is to explore the potential of this method to determine the provenance of archaeological artifacts. This investigation aims to identify similar spectral characteristics between the archaeological pieces and geological samples used as references for specific geological contexts.

To summarize, the accurate description and characterization of the raw materials employed in crafting items can

open an interesting line of research on commercial contacts among populations, shedding light on sources of supply and the socioeconomic models associated with them. Moreover, this approach could play a significant role in elucidating the functionality and symbolic and social value of certain materials over time.

Materials and methods

Materials

In the present study, we focus on the analysis of the spectral curves extracted from two archaeological pieces composed of black talc (Fig. 1).

Both pieces were found in the archaeological site of Peña del Castro (La Ercina, León) in the northwestern Iberian Peninsula, an Iron Age site dating from the tenth century BC until the change of era when the Roman conquest of the northern Iberian Peninsula destroyed the settlement (González Gómez de Agüero et al. 2015, 2018). The talc materials date from the last phase of occupation, between the second and first centuries BC. This was the period of greatest development of the settlement, which presented a high population density and a very complex society and economy, with intense commercial activity in both the main Plateau (Meseta) in the Central Iberian Peninsula and the Cantabrian Mountains in the northern area (González Gómez de Agüero et al. 2022). The talc documented at this site was found in both raw and processed forms and used to create spindle whorls and necklace beads.

We compared the spectral curves of the two studied pieces with those measured from the 50 geological samples classified as talc: 37 from outcrops near the studied archaeological site (called La Respina, San Andrés, and Mojón de las Tres Provincias outcrops), 12 from different places on the Iberian Peninsula, and 1 from a different geographical

area in Austria. We collected these geological samples (i) directly from old mining areas or outcrops or (ii) transferred them from the collections of the Spanish Geological Museum (Museo Geominero de España) and the Natural History Museum (Museo de Historia Natural) at the University of Santiago de Compostela. We organized and sorted all samples in the lithotheque from the lithic resources of the Prehistoric Laboratory at the University of León (Herrero-Alonso et al. 2018). This large number of samples from different geographical sources (Fig. 2 and Supplementary Table S1) enabled the generation of a spectral library presenting great variability in the talc spectral responses.

Finally, to ensure the mineralogical composition of the 52 samples, we compared their spectral curves with those from the US Geological Survey (USGS; Clark et al. 2016) and the NASA Jet Propulsion Laboratory (JPL) spectral libraries (Grove et al. 1992; Kokaly et al. 2017) using ENVI software.

Spectral data acquisition

The spectral measurements were performed using a spectroradiometer ASD FieldSpec-4 Standard-Res (Analytical Spectral Devices, Inc., Boulder, CO, USA). This covered a wavelength range from 350 to 2500 nm with spectral resolutions of 3 nm (350–1000 nm) and 10 nm (1000–2500 nm). As a result, we were able to capture reflectance responses at 2551 bands. These measurements need to be compared with diffuse reflection standards to minimize the uncertainty arising from the fact that no surface reflects all incoming radiation or is fully Lambertian. Therefore, to calibrate these outcoming reflectance values, we used a Spectralon 99% diffuse reflectance standard as a white reference, showing the least spectral variation (Ferrero et al. 2012).

We used a 2 cm diameter contact probe containing a light source (Supplementary Fig. S2) to avoid distortion of the spectral curve caused by the atmosphere. We fixed

Fig. 1 Archaeological pieces under study: (**a**) broken sample and (**b**) complete sample, both from the archaeological site of Peña del Castro (La Ercina, León)
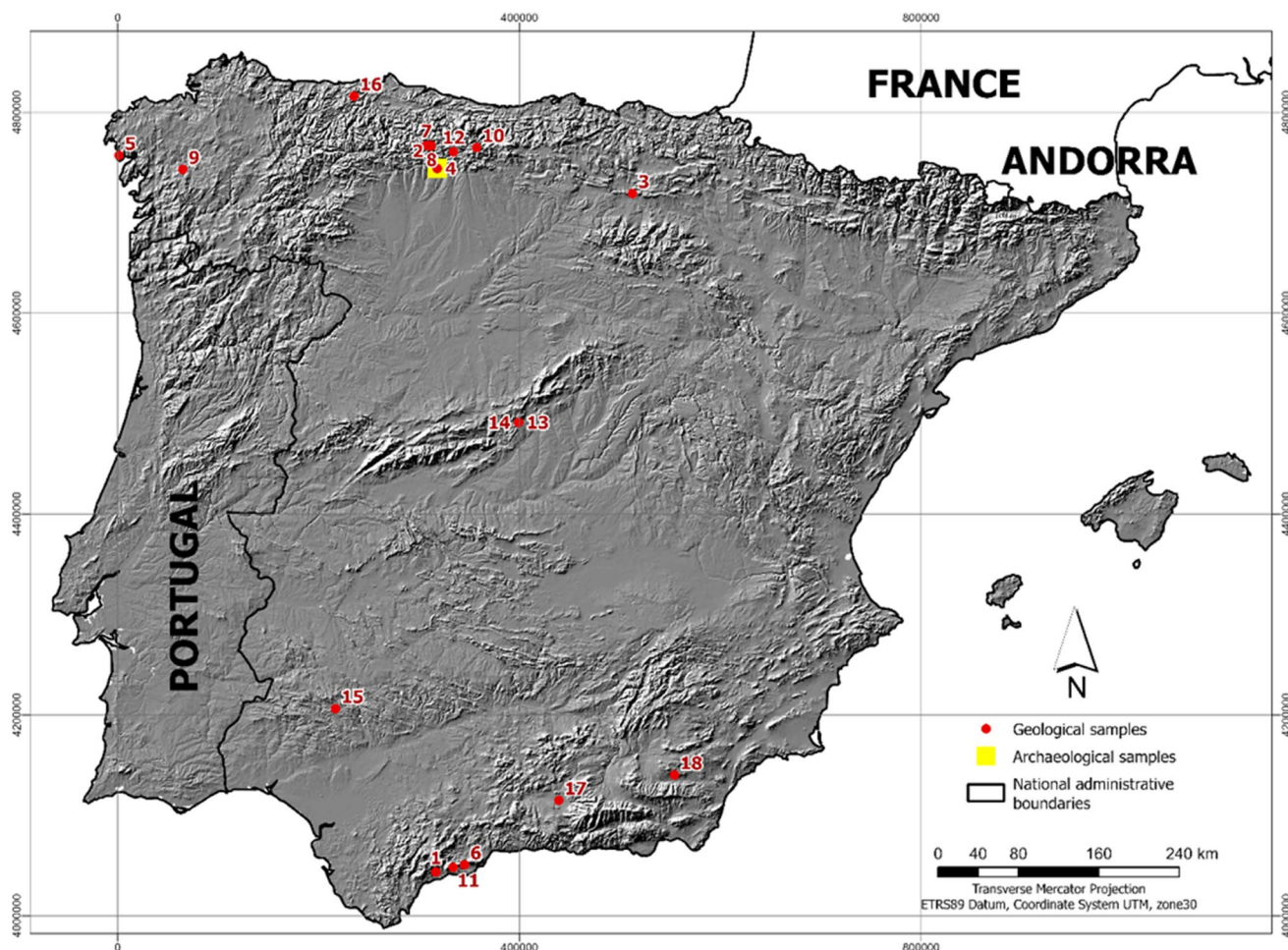
Fig. 2 Sample location

this contact probe vertically so that all measurements were recorded at the same angle. For rock analysis, this approach could present the issue of recording measurements on curved or small surfaces. In these cases, part of the electromagnetic energy was reflected outside the receiving field of the contact probe itself, altering the spectral response. For this reason, we measured the flattest surfaces of the rocks.

The number of measurements recorded for each sample varied according to the intended purpose, but in all cases

each measurement corresponded to the average of 15 internal spectral curve measurements. To study the suitability of this method to combine both powdered and bulk samples, the number of measurements was 15 in most samples. Multiple spectral measurements enable a better definition of the diagnostic spectral features (Kruse 2008). In this case, our analysis focused on six rocks from northern Spain, the only ones presenting both types of samples (Table 1). As the powdered samples presented a small quantity of available material, we measured them in a special recipient with a 2.5 cm

Table 1 Number of measurements and provenance of the powdered and bulk samples used to analyze the capability of the method to work together

	VDR02	MRE12	MJP06	MJP10	MJP11	237	Total
Powdered sample	12	15	15	15	15	15	87
Bulk sample	15	15	15	15	15	14	89
Location	Valderrodero (Asturias)	Mina La Respina (León)	Mojón de las Tres Provincias (León)	Mojón de las Tres Provincias (León)	Mojón de las Tres Provincias (León)	Haro (La Rioja)	

diameter surface and millimetric depth. We stirred the material before each measurement to guarantee independence.

To analyze the provenance of the archaeological pieces, we used the 52 samples. For this purpose, the number of measurements recorded from each bulk sample was three in most cases, considering their appearance variability (i.e., fresh cut or not; Table 2). Nevertheless, some bulk samples were too small, and we were able to perform only one or two measurements to ensure the correct angle and avoid outside reflection from the probe field. For powdered samples, we

Table 2 Sample types and number of measurements performed for mineralogical and geographical provenance analysis

Sample type		No. samples	No. measurements
Archaeological	Whole piece	1	4
	Broken piece	1	2
Geological	Powdered sample	22	25
	Bulk sample	23	64
	Both types of samples	5	21
Total		**52**	**116**

performed only one measurement per sample after confirming the homogeneity of their results in the first analysis.

For the archaeological pieces (Fig. 1), we also performed measurements at different positions of the object to cover all possible mineral variability due to chemical alteration: external/internal area, with/without drawings.

Spectral data analysis

Figure 3 shows an overall summary of the different spectral data analyses performed to achieve our objectives.

Data preprocessing

For spectral curve analysis, the spectral curved needed to be normalized for comparison. This normalization process is known as continuum removal. Several methods can be used to perform this process; convex and segmented hulls are the most common. In the present work, we normalized the spectral curves by continuum removal transformation, for which we considered the segmented hull (Clark et al. 1987), as this can identify small absorption features. Unlike the convex hull, the segmented hull could be concave as
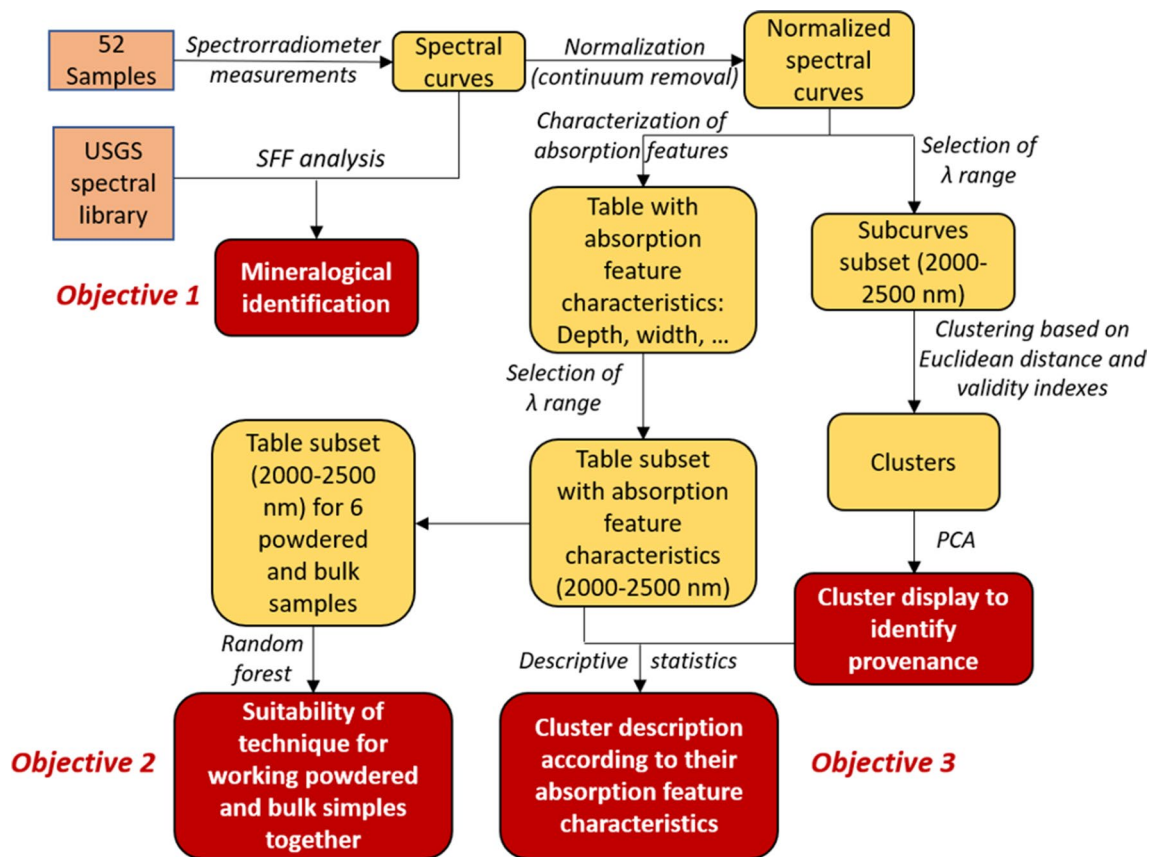

Fig. 3 Flow chart with the method followed to achieve the three objectives proposed in this study

long as the sign of its slope remained positive "before" the maximum and negative "afterwards."

For all curves, we manually selected the absorption features and subsequently characterized them by calculating their area, depth and corresponding wavelength, asymmetry, and full width at half depth (FWHD; Fig. 4). We performed these analyses—including segmented hull continuum removal—with the *hsdar* package (Lehnert et al. 2019) in R version 4.1.0 (R Core Team 2021).

Talc ($Mg_3Si_4O_{10}(OH)_2$) is a phyllosilicate mineral and, together with other minerals such as clays, can be identified by its absorption features located within the short-wave infrared (SWIR) region (Clark et al. 1990). Talc comes from the alteration of silicates rich in magnesium, such as olivine or pyroxene and amphiboles (Klein and Hurlbut 2008), which are mainly altered by hydrothermal processes on dolomite and magnesite (Chung et al. 2020). Magnesite is associated with carbonate rocks, where talc is an accessory mineral together with calcite and dolomite. Since all these minerals usually appear together after hydrothermal processes, the complexity of spectroscopic analysis increases (Chung et al. 2020). All these minerals show absorption features in the 2300 nm proximities, although some small differences may enable their recognition (Supplementary Fig. S3); dolomite and calcite show characteristic features at 2320 nm and 2340 nm, respectively, and magnesite and talc shift towards 2300 nm. Despite this coincidence between these last two minerals, talc can be distinguished by its triple feature near 2077/2127/2172 nm that appears in high-quality cosmetic talc (Pi-Puig et al. 2020). This type of powder sample needs to contain more than 90% talc (Delgado et al. 2020). As in other minerals, a large feature appears at 1910 nm, which
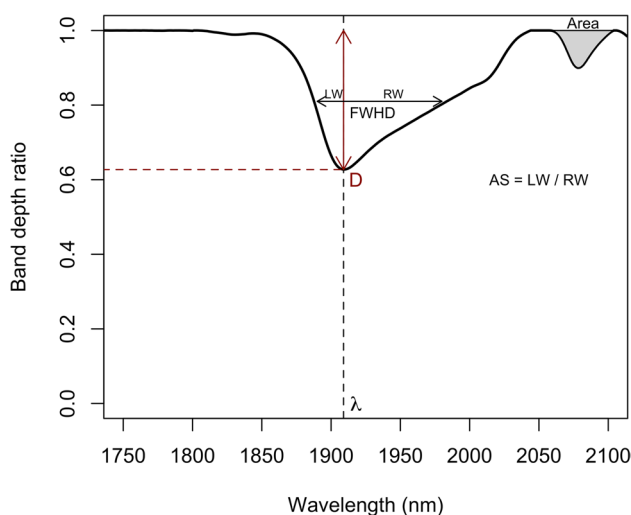
originates in the presence of water, and at 1400 nm, with the presence of OH^-.

As the most characteristic absorption features of the talc fall in the SWIR interval of 2000–2500 nm, in the present study, we focus on these features when analyzing the data, except for the identification of the sample's mineralogy, for which we examine the entire interval.

Equivalence between powdered and bulk rock samples

We used the measurements from the six geological powdered and bulk samples (Table 1) to evaluate the influence of sample type on the analysis of spectral curves and thus to assess the suitability of working with both sample types in the same study (the second objective of the present paper). We used a random forest as it is a supervised learning problem. Random forest is a machine learning algorithm that enables the prediction of the class (here, the sample) from the observed variables (here, the absorption feature characteristics) of new data. The available data are classified and divided into the training sample and the validation sample. The algorithm fits several decision trees with random samples taken from the training sample and predicts the class of the validation sample. The random forest selects the class with the highest number of votes from the decision trees and uses the known class of the validation sample to calculate the accuracy of the model (Castiello and Tonini 2021).

Note the feature characteristics (depth and area) always take nonnegative values, which implies that their distribution will most likely be asymmetric. Moreover, these are variables likely to be correlated. Unlike other supervised learning techniques such as linear discriminant analysis, random forests do not require the distribution of the variables to be normal or the homogeneity of variances.

We trained a random forest model with all data and estimated classification errors. Specifically, we grew 500 trees, each predicting one randomly selected case called out-of-bag (OOB). We estimated the OOB error of the random forest with the percentage of the misclassified cases. We used the *randomForest* R package (Liaw and Wiener 2002) for the forest analysis. The analysis included several variables and their combinations, and we selected the predictive variables according to the classification errors and the model's parsimony.

The results of this analysis determine whether provenance study of archaeological pieces should rely solely on information extracted from bulk samples or powdered samples can also be included (Table 2).

Mineralogical identification with spectral feature fitting

We incorporated the 116 spectral curves of the 52 samples into a spectral library in the ENVI software and compared

Fig. 4 Characterization of the spectral data by their area, depth (D) and corresponding wavelength (λ), asymmetry (AS), and full width at half depth (FWHD)

them with the USGS and JPL spectral libraries based on the spectral feature fitting (SFF) method. This is a well-known approach in hyperspectral analysis that compares each spectral curve of the samples with the different spectral curves of the general spectral libraries and identifies the mineral substances according to least squares fitting algorithms (Jain and Sharma 2019). A result closer to 1 correlates to a higher probability of correspondence between the spectral curve of the sample and that of the known mineral. These results enabled the identification of those samples that were initially miscatalogued as talc in the museums.

Study of archaeological pieces' provenance

To determine the provenance of the archeological pieces we used a clustering algorithm. Clustering is a machine learning algorithm for unsupervised classification that divides a sample (not previously classified) into k homogeneous subgroups by maximizing the differences among groups. Usually, the number of groups or clusters, k, needs to be determined by the user (Schmidt et al. 2022).

One of the most effective machine learning methods for unsupervised learning is k-means; however, this is sensitive to the initial selection of cluster centers (Chen et al. 2005). To avoid this problem, we used hierarchical k-means clustering, a hybrid approach that combines hierarchical clustering (for centers initialization) and k-means methods, implemented in the *factoextra* R package (Kassambara and Mundt 2020). We determined the number of clusters considering several internal validity indices (silhouette, Dunn, within sum of squares). We used a hierarchical k-means clustering, with the Euclidean distance method, of the 2000–2500 nm wavelength range of the curves to approach this problem, using the curve instead of just feature characteristics. We selected the agglomeration method that minimized the within-cluster sum of squares. We use principal component analysis to display the clustering results.

Results

The visual analysis of the spectral curves enabled the absorption features to be distinguished around different wavelengths (Table 3). Not all features appeared in all samples, and previous literature did not show a unique common number of absorption features. These differences were the result of the nonpure talc samples; however, talc was also mixed with other mineralogical compositions that absorbed energy at other wavelengths.

We obtained absorption features at the following wavelengths (nm): 1271, 1827, 1910, 2000, 2080, 2140, 2180 (where these last three wavelengths corresponded to a triple feature described by Pi-Puig *et al.*, 2020), 2230, 2312 (where both wavelengths corresponded to a doublet-shaped pattern described by Bhadra *et al.*, 2020), 2380, 2430, 2470, and 2488. However, these wavelengths did not appear in all the samples' spectral curves: some repeatedly appeared in more than 80% of the examined curves, such as those at 1910 and 2312 nm (Table 3), and others sporadically appeared, such as the absorption features at 2430 or 2488 nm. The two shallow absorption features near 2456 nm could appear in talc rocks that were influenced by the FeMg-OH contents in the sample (Basavarajappa et al. 2020).

Talc is an active SWIR mineral (Govil et al. 2017); thus, for the analysis of the absorption feature characteristics, we only used those features in the SWIR that presented a low–medium number of missing data. Therefore, the following wavelengths corresponding to the absorption features were selected as characteristic of the talc spectral curves: 2080, 2140, 2180, 2230, 2312, 2380, and 2470 nm. All matched those observed in the USGS library, except the one at 2285—2290 nm that did not appear in the samples of the present study and was a minor absorption feature in several previous works (Chung et al. 2020; Clark et al. 1990; Govil et al. 2017; Laukamp 2011, or in the USGS library). This feature is associated with the presence of Mg-OH (Jain et al. 2022).

Table 3 Comparison of the wavelengths for the talc absorption features among the present study results and different authors starting at 1900 nm

Author	Wavelength (nm)											
Present study	1910	2000	2080	2140	2180	2230	—	2312	2380	2430	2470	2488
Chung *et al.*[1]	1910	2010	2077	2133	2172	2233	2290	2311	2383	—	—	—
Clark *et al.*[2]	—	2010	2077	2133	2172	2233	2285	2311	2383	—	2470	—
Govil *et al.*[3]	1905	—	—	—	—	2245	2285	2315	2386	—	—	—
Laukamp[4]	—	—	2077	2127	2172	—	2279	2300	2380	—	—	—
% of available data	81%	17%	**78%**	**53%**	**39%**	**77%**	0%	**97%**	**71%**	7%	**83%**	3%

[1]Chung et al. (2020)
[2]Clark et al. (2016)
[3]Govil et al. (2017)
[4]Laukamp (2011)

Comparison between powdered and bulk rock samples

Not all curves presented the same number of absorption features or features at the same wavelengths (Table 3). When data are missing, the random forest analysis requires data imputation before model fitting. Here, this process was simple: the area could be considered 0 and the depth and asymmetry needed to 1 when no feature was present at a given wavelength.

To run a random forest analysis, the first step was variable selection. Initially, we considered the wavelength position of the feature, the feature depth, the full area, and the absorption band asymmetry, as the FWHD provided redundant information due to the previous choice of depth and area. As a result, depth provided the lowest OOB error (3.41%), followed by area (4.55%), and asymmetry (10.8%); this result showed a similar performance to the analysis performed using the three variables (3.41%). Therefore, depth appeared to be the most significant absorption feature characteristic to classify the powdered and bulk samples with random forest. This result was expected, as this was an indicator of the amount of the material causing the absorption present in a sample (van der Meer 2004). From the random forest classification, the most important features' depths were located, in order of importance, at approximately 2230, 2180, 2080, 2312, and 2140 nm.

Following the analysis of the 87 powdered and 89 bulk rock samples, we generated the confusion matrix of the trained random forest with its corresponding classification errors (Table 4).

This result, together with the low OOB error estimation, indicates that both types of samples present similar spectral curves. Among all samples, the MJP11 samples show the main errors, but most of the incorrect allocations were assigned to other samples (MJP06 and MJP10) found in the same geographical location. Although these could show different alteration degrees due to different hydrothermal processes, samples from closer sources were expected to show more similar spectral curves.

Internally, when the different spectral curves measured from a unique sample were compared, the high homogeneity of the data was remarkable. As shown in Fig. 4, this homogeneity was higher in powdered than in bulk rock samples, but, in both cases, the absorption features were the same. The top panel in Fig. 4 with the raw data shows the main differences; these differences were related to the amount of reflected energy (overall reflectance). The powdered samples showed values between 0.3 and 0.75, while the reflectance data in bulk rock samples were always lower than 0.3. Remarkably, in powdered samples, the reflectances in the 1500–1900 nm interval were higher than those in wavelengths under 1500 nm, while in bulk rock samples, the reflectances were similar. Finally, differences in the absorption features located in the interval of 2000–2300 nm were observed. The powdered samples showed the triplet feature absorption with similar minimum reflectance values; however, in the bulk rock samples, these minimum values decreased as the wavelength increased. All these differences disappeared upon normalization of the data with the continuum removal (bottom panel in Fig. 5). In this case, the main differences between powdered and bulk rock spectral curves were the depth and the area of the different spectral features. In any case, the standard deviation (SD) values were low (Table 5), and the sum of square errors (SSE) ratio of powdered over bulk measurements was high due to the extremely low values of the powdered measurements.

Identification of the non-talc samples

According to the SFF analysis, only 2 spectral curves from the 116 analyzed did not fit a high SFF score for the talc spectral curve. The first sample was a green powdered sample from Riaño (León, Spain). SFF enabled its identification as dickite (Fig. 6), with a similitude score of 0.9. The spectral curve of this mineral was characterized by several double-shaped absorption features, with two being most relevant by their depth. The first was the double absorption feature at 1378–1383 and 1412–1414 nm. The second double absorption was located in the SWIR, at 2175–2180

Table 4 Confusion matrix for random forest after training

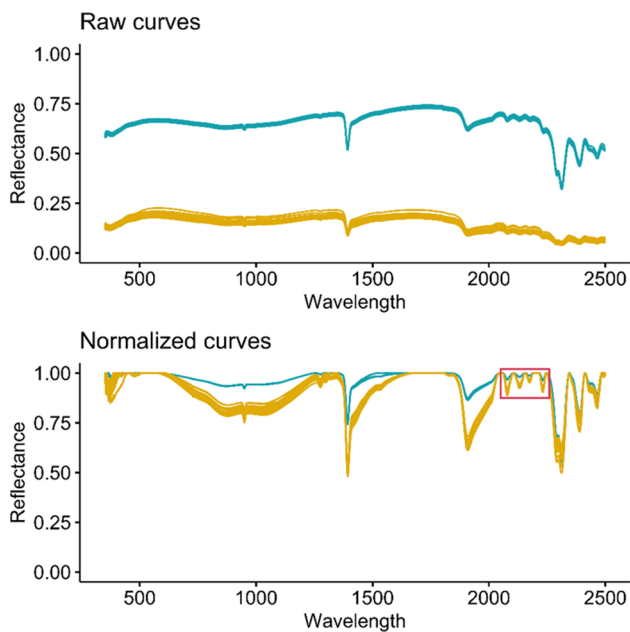| Estimated sample							
	VDR02	MRE12	MJP06	MJP10	MJP11	237	Classification error
VDR02	27	0	0	0	0	0	0.00
MRE12	0	30	0	0	0	0	0.00
MJP06	0	0	30	0	0	0	0.00
MJP10	0	0	0	30	0	0	0.00
MJP11	0	1	2	2	24	1	0.20
237	0	0	0	0	1	28	0.03

Fig. 5 Reflectance curves from the powdered (blue) and bulk (yellow) rock samples named MJP06: raw data (top); data after continuum removal (bottom). Wavelengths corresponding to the depths of the most important features appear inside the red square in the normalized graph

Table 5 Standard deviation (SD) and SSE ratio values for powdered and bulk rock samples with raw and normalized data for the MJP06 sample

	Sample type	SSE ratio of powdered over bulk	SD	SD range
Raw	Powdered	5.05	0.005	0.004–0.006
	Bulk		0.011	0.006–0.013
Normalized	Powdered	33.02	0.001	$2\cdot10^{-8}$–0.007
	Bulk		0.010	$2\cdot10^{-8}$–0.041

and 2200–2205 nm. This small shift in the wavelengths of the absorption features corresponded to the different spectral library sources. Several representative single-absorption features were also observed, such as a wide feature that ranged between 1756 and 1855 nm and correlative features at 2305, 2355, 2383, and 2439 nm. Subsequent X-Ray diffraction (XRD) analysis confirmed this mineralogy. Physical properties that could have led to the misclassification of this material were potentially related to its color and ease of carving.

The second sample that showed low fitting with the talc spectral curve was the spectral curve called VDR02. VDR02 is a green sample used in a previous study (Section "Comparison between the powdered and bulk rock samples".) of equivalence between powdered and bulk rock samples; however, due to the evidence of high correspondence fitting

between powdered and bulk rock, only the powdered sample was analyzed to define its mineralogy. This sample came from Valderrodero (Asturias, Spain). Although the spectral curves of the JPL spectral library did not show any correspondence with these sample curves, those from the USGS library showed a relatively high SFF score with clinochlore and chlorite (Fig. 7). The three spectral minerals showed very similar fitting scores (Table 6). Two corresponded to clinochlore and one to chlorite. Clinochlore is the Mg-rich trioctahedral species in the chlorite group (Bishop et al. 2008); for this reason, this was considered a coherent SFF result.

Archaeological sample provenance analysis

Since no evidence was found of powdered and bulk rock samples presenting essential differences in their spectral curves, we considered the complete dataset of talc samples to assess the validity of the spectral curve analysis in determining the samples' provenance. For this purpose, we performed hierarchical k-means clustering considering three groups (following the silhouette index, which clearly recommends this number of clusters). The results are shown in Figs. 8 and 9 and Table 7.

As shown in Fig. 8, Cluster 3 was more homogeneous than the other two clusters, in which their measurements were more spread over the graph. These measurements did not correspond to actual location of the samples from a specific place, which raised doubts regarding the adequacy of this method to determine the provenance of the samples. Remarkably, the spectral curves from the broken archaeological sample were classified in a different cluster than those from the entire archaeological sample. Moreover, the measurements from the unbroken archaeological sample were spread over Clusters 1 and 2, although these were closely located in the two-dimensional graph (Fig. 8).

Differences in clusters' inner homogeneity are shown in Fig. 9. The highest variety was found in the absorption feature at approximately 2230 nm in Cluster 1, although this feature did not sufficiently represent the spectral curves of this cluster because this was not reflected in the mean spectral curve. Comparing the three clusters' mean spectral curves, all three showed absorption features at the same wavelengths, although with different characteristics. Cluster 2 showed low depth at their absorption features, while Cluster 3 presented the deepest absorption features. In addition, the triplet feature absorption of Cluster 3 did not reach the maximum value upon normalization of the spectral curve, while those for Clusters 1 and 2 did reach the maximum upon normalization. Therefore, when automatizing the characterization of the absorption features in the case of Cluster 3, the triplet was considered a unique feature, while in

Fig. 6 Spectral curves of the dickite samples after continuum removal operation: bulk rock sample's spectral curve number 35 from Riaño (León, Spain) in green, two samples from the USGS library (Kokaly et al. 2017) in red (named NMNH46967) and dotted orange line (named NMNH106242), and a sample from the JPL library with < 45 micrometer grain size in blue
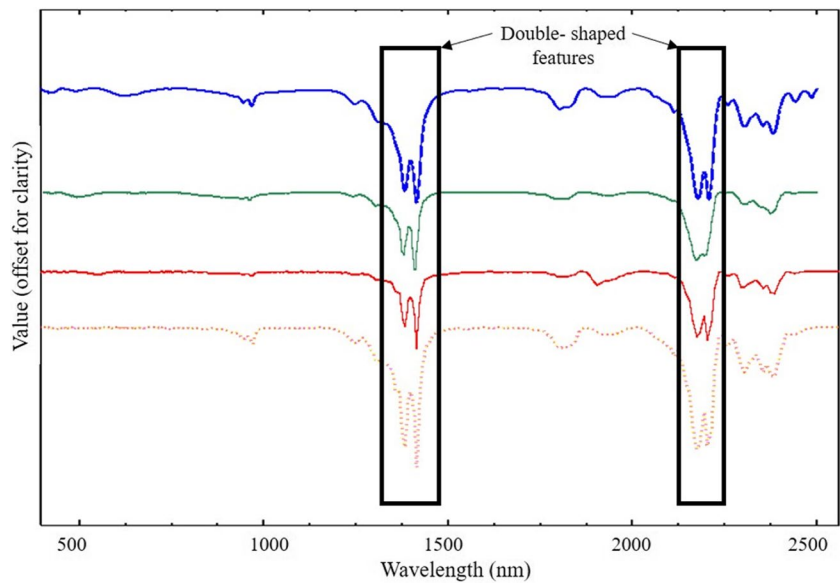

Fig. 7 Spectral curves of chlorite and clinochlore of the USGS library (Kokaly et al. 2017) showing a high SSF score with sample VDR02 (in purple). Cchlore3.spc curve appears in green, Cchlore1.spc in red and Chlorit3.spc in blue
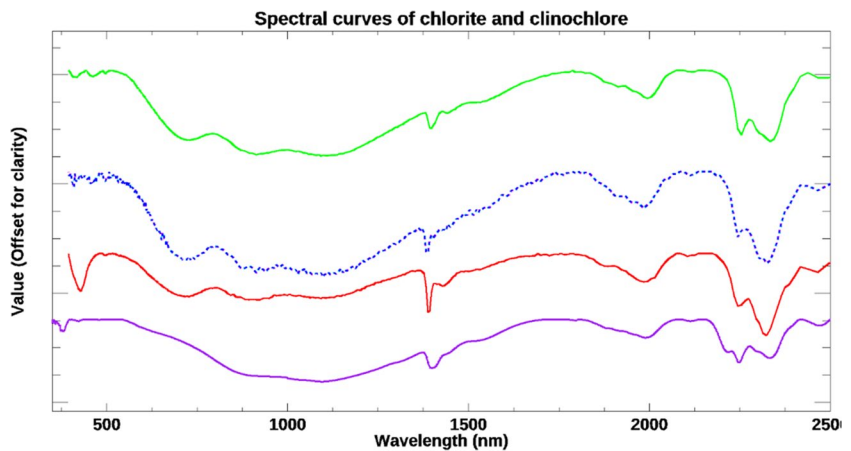
Table 6 SFF scores of the VDR02 sample with spectral curves from the USGS library

Spectral curves				
	Study	USGS		
Sample	*Number*	*Cclore1*	*Chlorit3*	*Cchlore3*
VDR02	Talc44.asd	0.711	0.708	0.703

Clusters 1 and 2, their triplets were considered three separate features.

The clusters confirmed the impossibility of identifying the sample's provenance, at least with this method (Table 8). Different samples from the same region were classified into different clusters. This result was expected in regions such as Andalucía or Galicia, where, although geographically unique, the samples belonged to different geological formations. However, this result was repeated in the samples from León, belonging to the same geological formation.

Discussion

During the macroscopic analysis of the recovered artifacts at Peña del Castro, these were initially described as possibly coming from the talcs that outcrop in the area of Puebla de Lillo (La Respina and San Andrés). However, as this was a visual method, a mineralogical study was necessary to confirm or reject this hypothesis. In the present work, we firstly confirmed that the remains from La Peña del Castro are indeed talc. This greatly limits the provenance of these materials since, as mentioned, the outcrops are more restricted. Furthermore, the different peaks of the archaeological talc samples could be characterized, allowing for comparisons with other materials.

The use of continuum removal is a well-known technique. The most common method is the convex hull (Mutanga and Skidmore 2004). However, the method used in the present study was the segmented hull to adapt to
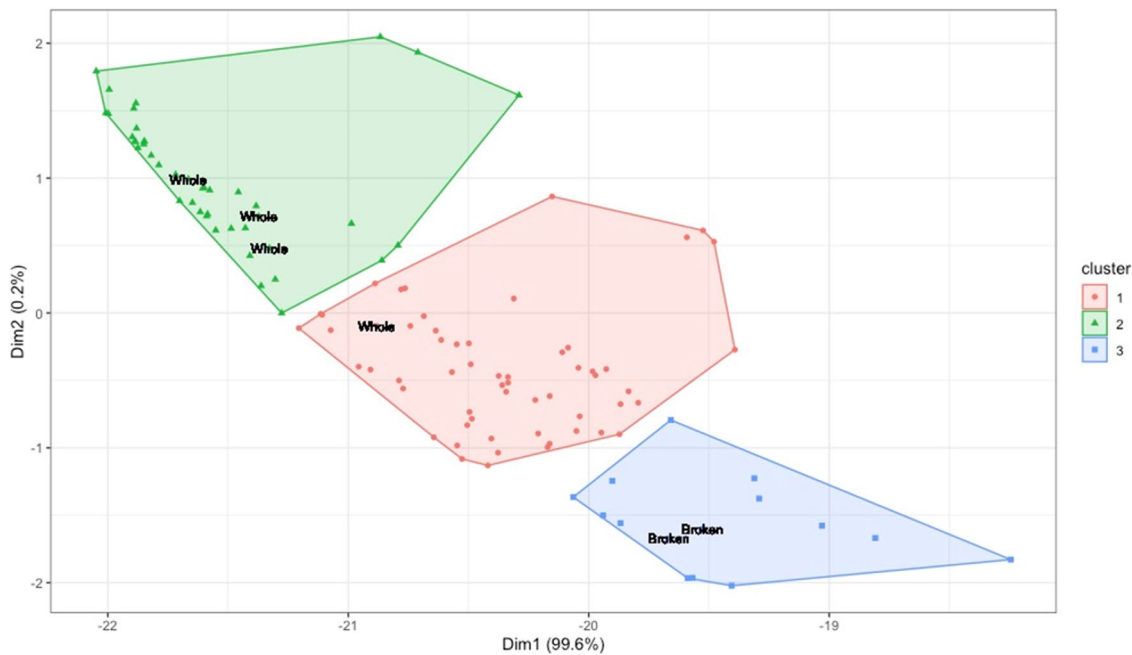
Fig. 8 Result of the classification considering three clusters. Archaeological samples labelled 'Whole' an'Broken'. Axes represent the values of the first two dimensions of the principal component analysis, allowing multidimensional data to be displayed in two dimensions
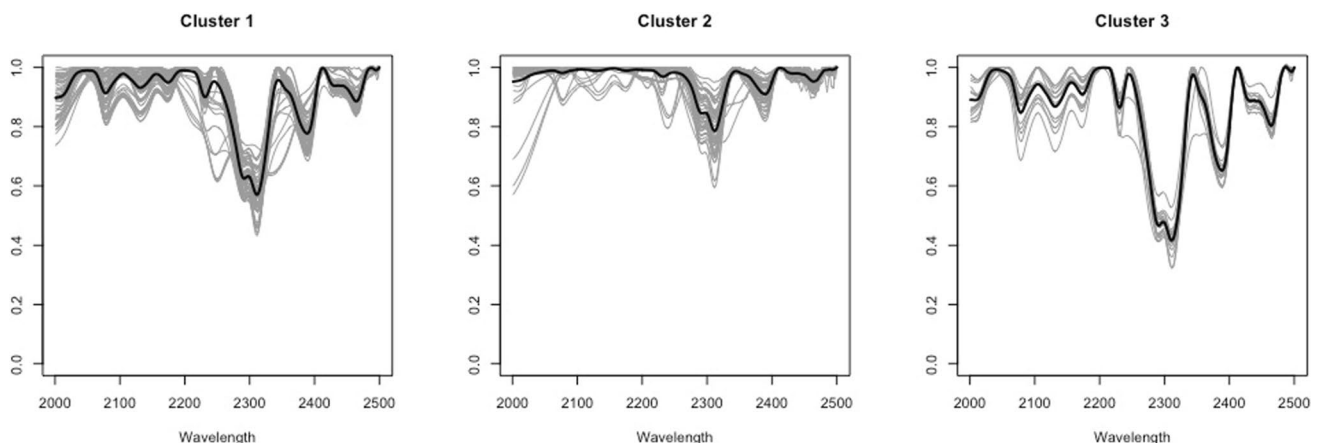

Fig. 9 Mean curves of each cluster superimposed over the individual curves corresponding to each cluster

those double- or triple-shaped absorption features. Some authors (Clark et al. 1987) view this method as the best one to identify small absorption features. Nevertheless, the results obtained in our study show that, although this method can be useful in some cases, this was not infallible, and not all the small absorption features that were visually observed by humans could be automatically identified by computers.

The rock samples of MJP06, MJP10, and MJP11 presented the same geographical location. Nevertheless, their spectral curves were perfectly assigned to the right group when comparing powdered and bulk rock spectral curves with the random forest classification. This represents a remarkable success, especially with MJP10 and MJP11 measurements. Different from MJP06, a green talc rock, these other samples were black talc rock. Color differences are related to talc purity. A linear decrease was observed between the whiteness and impurity minerals (Togari 1979); thus, different minerals were expected to show their footprint in the spectral curve. While green talc showed the presence of chlorite minerals in the dark talc, its color was derived from the organic matter content (Pi-Puig et al. 2020). Therefore, chlorite impurities could facilitate the discrimination of MJP06 from the rest. MJP10 and MJP11, extracted from the

Table 7 Characterization of absorption features of talc between 2000 and 2500 nm

		Cluster 1	Cluster 2	Cluster 3
2080 nm	*Depth*	0.90 ± 0.05	0.98 ± 0.03	0.84 ± 0.07
	Area	4.92 ± 5.27	1.1 ± 2.84	10.2 ± 8.19
	Asymmetry	0.56 ± 0.31	0.8 ± 0.3	0.41 ± 0.29
2140 nm	*Depth*	0.95 ± 0.03	0.98 ± 0.02	0.92 ± 0.03
	Area	1.99 ± 1.71	0.51 ± 0.66	3.17 ± 2.22
	Asymmetry	0.97 ± 0.72	0.85 ± 0.24	1.14 ± 1.02
2180 nm	*Depth*	0.97 ± 0.02	0.99 ± 0.01	0.95 ± 0.00
	Area	0.46 ± 0.29	0.22 ± 0.44	0.83 ± 0.08
	Asymmetry	1.05 ± 0.11	1.21 ± 0.76	1.03 ± 0.06
2230 nm	*Depth*	0.89 ± 0.08	0.96 ± 0.06	0.87 ± 0.04
	Area	5.44 ± 14.3	1.13 ± 2.05	1.95 ± 0.65
	Asymmetry	0.93 ± 0.24	1.24 ± 0.62	1.01 ± 0.11
2312 nm	*Depth*	0.56 ± 0.07	0.79 ± 0.07	0.41 ± 0.05
	Area	26.3 ± 8.47	10.7 ± 3.77	35.8 ± 9.03
	Asymmetry	1.84 ± 0.63	2.02 ± 0.42	1.70 ± 0.72
2380 nm	*Depth*	0.77 ± 0.04	0.90 ± 0.03	0.65 ± 0.05
	Area	8.05 ± 2.16	3.21 ± 1.22	13.5 ± 2.32
	Asymmetry	1.62 ± 0.43	1.60 ± 0.41	1.42 ± 0.49
2470 nm	*Depth*	0.88 ± 0.04	0.95 ± 0.02	0.79 ± 0.02
	Area	4.41 ± 1.55	1.84 ± 0.80	8.23 ± 1.07
	Asymmetry	2.87 ± 0.99	2.09 ± 1.50	3.82 ± 0.84

Table 8 Provenance of samples in each cluster

Provenance		Cluster 1	Cluster 2	Cluster 3
Andalucía		10	0	4
Asturias		3	0	0
Austria		0	0	2
Galicia		1	1	0
La Rioja		2	3	0
León		40	33	7
	Puebla de Lillo	1	2	0
	Mina de la Respina	17	6	3
	Mina de San Andrés	10	6	0
	Mina de las Tres Provincias	12	19	4
Madrid		1	3	0

same source, could potentially show a similar influence of the organic matter content in the spectral curve, challenging their classification; however, this did not occur.

The incorporation of a non-talc sample (VDR02) in the powdered-bulk spectral analysis enabled the identification of a different mineral composition from the rest of the talc samples. Mixing of different mineralogical pieces often occurs in archaeological collections due to the similarities in color and softness. In addition, talc deposits usually appear in the

field accompanied by carbonates, chlorite, and some quartz, which can hinder the correct identification by nonexperts in mineralogy. Therefore, if a previous talc sample has been extracted from the nearby area, the classification of future samples may be assigned to the same mineral composition without close examination. Talc and clinochlore are SWIR active minerals and share some absorption features, such as (approx.) 2075 and 2235 nm (Govil et al. 2017). However, these show different diagnostic absorption features. While clinochlore shows these features at 2255 nm and 2315–2345 nm due to the vibrational processes of AlFe-OH or AlMg-OH and MgOH (Govil et al. 2017), talc shows these features at 2315 and 2386 nm together with shoulder absorption features at 2285 nm and 2245 nm (Govil et al. 2017). For this reason, although visual characteristics may lead to incorrect mineral identification, the use of spectroscopy can easily allow a quick distinction.

The technique presented herein shows some limitations. Regarding data acquisition, spectroscopic measurements require an effective surface area larger than 1.5 cm in diameter; thus, not all archaeological pieces are suitable for analysis. Machine learning methods, such as the *k*-means clustering used here, require large sample sizes and strongly depend on the representativeness of the data used. Our analysis was applied to a medium-size convenience sample set, and the spectral curves of the same geographical region did not show homogeneity. Although these limitations were present, our results show that the proposed method was not decisive in establishing the provenance of the archaeological pieces. Inside a geological formation, different mineralogical compositions appeared in the same lithological unit, for example, due to different alteration processes, which hindered the identification of the provenance of a sample. Therefore, the fact that the archaeological pieces were in different clusters could indicate a mineralogical difference between the two pieces; however, this result was not decisive to affirm that these came from two different geographical points.

All these limitations are largely outweighed by the benefits of our presented method. In addition to allowing mineral identification, this technique presents the advantage of nondestructive sampling; thus, this can be applied to all archaeological materials. Moreover, this is a portable technique that enables work in facilities outside the laboratory, such as museums. This technique is also economical, since this does not require consumables, and fast, since numerous measurements can be obtained in a few minutes.

Conclusions

Presence of soft minerals was common in deposits in our study area from various periods, and these minerals were generally identified as talc. Their use tended to be

ornamental, although not exclusively. As these archaeological pieces are unique, these should not be destroyed for analysis; thus the difficulty to examine them and the limited analytical techniques that can be applied. Reflectance spectroscopy enabled the identification of the mineralogical composition of the samples, allowing a better definition of the raw materials used by past human societies. We were not able to discriminate among the different sources of supply in the present study with this nondestructive technique. However, we obtained valuable information regarding the possibility of local or exogenous materials since these could not be found near settlements. This fact, together with the macroscopic analyses, can represent an important tool in defining the trade and mobility aspects of prehistoric human groups.

Moreover, since our results were similar for both powdered and whole samples, this technique shows great value and potential. Given that archaeological materials cannot be analyzed with high precision, at low cost, quickly, cheaply, comparably, and, perhaps most importantly, without the need to destroy the pieces, this technique can be useful to study materials located in archaeological sites, museums, and deposits as the samples do not need to be removed from their location due to the portable nature of the equipment required for the analysis.

Finally, the application of this method represents an important contribution to archaeological studies even though the provenance of the materials cannot currently be identified and a descriptive rather than analytical technique is used. Therefore, further research is needed utilizing these techniques and combining them with others to enable their use to achieve more ambitious goals.

Declarations

References

Basavarajappa H, Abrar A, Manjunatha M (2020) Hyperspectral and geochemical signatures study of indutrial steatite deposit around Bhahaddurghatta-Hosahatty village of Chitradurga Taluk, Karnataka, India. Int J Eng Res Mech Civil Eng 5(2):14–22

Bhadra BK, Pathak S, Nanda D, Gupta A, Rao SS (2020) Spectral characteristics of talc and mineral abundance mapping in the Jahazpur Belt of Rajasthan, India using AVIRIS-NG data. Int J Remote Sens 41(22):8757–8777. https://doi.org/10.1080/01431161.2020.1783710

Bishop JL, Lane MD, Dyar MD, Brown AJ (2008) Reflectance and emission spectroscopy study of four groups of phyllosilicates: smectites, kaolinite-serpentines, chlorites and micas. Clay Miner 43(1):35–54. https://doi.org/10.1180/claymin.2008.043.1.03

Bruni S (2022) Etruscan Fine Ware Pottery: Near-Infrared (NIR) Spectroscopy as a Tool for the Investigation of Clay Firing Temperature and Atmosphere. Minerals 12:412. https://doi.org/10.3390/min12040412

Castiello ME, Tonini M (2021) An explorative application of random forest algorithm for archaeological predictive modeling. a swiss case study. J Comput Appl Archaeol, https://doi.org/10.5334/jcaa.71

Celis Sánchez J (2007) En los límites noroccidentales del territorio vacceo. In: Sanz Minguez C, Romero Carnicero F and Celis Sánchez J (Eds.) En los extremos de la región vaccea, Caja España, León, pp 43–58

Celis Sánchez J, Grau Lobo L (2007) Un oppidum en el valle del Cea: Los Castros de Villamol. In: C. Sanz Minguez, F. Rosemary Butcher y J. Celis Sanchez (Eds.) En los extremos de la región vaccea. León: Caja España, pp 81–82

Cheilakou E, Troullinos M, Koui M (2014) Identification of pigments on Byzantine wall paintings from Crete (14th century AD) using non-invasive Fiber Optics Diffuse Reflectance Spectroscopy (FORS). J Archaeol Sci 41:541–555. https://doi.org/10.1016/j.jas.2013.09.020

Chen B, Tai P, Harrison R, Pan Y (2005) Novel hybrid hierarchical-K-means clustering method (H-K-means) for microarray analysis. In: 2005 IEEE Computational Systems Bioinformatics Conference - Workshops (CSBW'05), pp 105–108. https://doi.org/10.1109/CSBW.2005.98

Chung B, Yu J, Wang L, Kim NH, Lee BH, Koh S, Lee S (2020) Detection of magnesite and associated gangue minerals using

hyperspectral remote sensing – A laboratory approach. Remote Sensing 12(8):1325. https://doi.org/10.3390/rs12081325

Clark RN, King TVV, Klejwa M, Swayze GA, Vergo N (1990) High spectral resolution reflectance spectroscopy of minerals. J Geophys Res : Solid Earth 95(B8):12653–12680. https://doi.org/10.1029/JB095iB08p12653

Clark R, King T, Gorelick N (1987) Automatic continuum analysis of reflectance spectra. Proceedings of the Third Airborne Imaging Spectrometer Data Analysis Workshop, pp 138–142. https://ntrs.nasa.gov/api/citations/19880004388/downloads/19880004388.pdf

Clark R, Swayze G, Wise R, Livo E, Hoefen T, Kokaly R, Sutley S (2016) USGS digital spectral library splib06a: U.S. geological survey, digital data series 231. Available online:http://speclab.cr.usgs.gov/spectral.lib06. Accessed 12 Jul 2016

Delgado R, Fernández-González MV, Gzouly M, Molinero-García A, Cervera-Mata A, Sánchez-Marañón M, Herruzo M, Martín-García JM (2020) The quality of spanish cosmetic-pharmaceutical talcum powders. Appl Clay Sci 193:105691. https://doi.org/10.1016/j.clay.2020.10569

Escortell M, Maya JL (1972) Materiales de "el pico castiello", Siero en el museo arqueológico provincial. Archivum Revista de la Facultad de Filosofía y Letras 22:37–48

Ferrero A, Rabal AM, Campos J, Pons A, Hernanz ML (2012) Spectral and geometrical variation of the bidirectional reflectance distribution function of diffuse reflectance standards. Appl Opt 51(36):8535–8540. https://doi.org/10.1364/AO.51.008535

Fischer C, Hsieh E (2017) Export Chinese blue-and-white porcelain: compositional analysis and sourcing using non-invasive portable XRF and reflectance spectroscopy. J Archaeol Sci 80:14–26. https://doi.org/10.1016/j.jas.2017.01.016

Galán-Huertos E, Rodas M (1973) Contribución al estudio mineralógico de los depósitos de Talco de Puebla de Lillo (León, España). Boletín Geológico y Minero, Tomo 84(5):45–63

García del Moral LF, Morgado A, Esquivel JA (2021) Reflectance spectroscopy in combination with cluster analysis as tools for identifying the provenance of Neolithic flint artefacts. J Archaeol Sci: Rep 37:103141. https://doi.org/10.1016/j.jasrep.2021.103041

González Gómez de Agüero E, Bejega García V, Muñoz Villarejo F (2015) El poblamiento castreño en la montaña leonesa. Férvedes Revista De Investigación 8:191–200

González Gómez de Agüero E, Bejega García V, Muñoz Villarejo F (2018) Las excavaciones en la Peña del Castro (La Ercina, León). Campañas de 2015 a 2017. Férvedes Revista De Investigación 9:97–106

González Gómez de Agüero E, Castañeira-Pérez N, Herrero-Alonso D, Ruano Posada L (2022) Las implicaciones del desarrollo de la agricultura durante la Edad del Hierro en el norte de la península ibérica: el caso de la Peña del Castro (La Ercina, León, España). Trab Prehist 79(1):85–98. https://doi.org/10.3989/tp.2022.12288

González Gómez de Agüero E, Ruano Posada L, Herrero Alonso D, Martín Seijo M (2023) La arquitectura de la Edad del Hierro en la zona cantábrica. El caso de La Peña del Castro (La Ercina, León). Complutum 34(2):499–526. https://doi.org/10.5209/cmpl.92266

Govil H, Gill N, Rajendran S (2017) Identification of talc and chlorite mineral in the askot crystalline of kumaon himalaya using hyperion hyperspectral data. In: 38th Asian Conference on Remote Sensing - Space Applications: Touching Human Lives, ACRS 2017 - New Delhi, India, Oct 23 2017-Oct 27 2017. Available at https://a-a-r-s.org/proceeding/ACRS2017/ID_5_749/286.pdf. Accessed Sep 2023

Grove C, Hook S, Paylor E (1992) Laboratory reflectance spectra of 160 minerals, 0.4 to 2.5 micrometers. Jet Propulsion Laboratory Publication 92–2. https://hdl.handle.net/2014/40148

Gutiérrez González JA (1986) Tipologías defensivas en la cultura castreña de la Montaña Leonesa. Zephyrus 39–40:329–335

Herrero-Alonso D, Fuertes-Prieto MN, Fernández-Martínez E, Gómez-Fernández F Alonso-Herrero E, Matero-Pellitero AM (2018) Legiolit: Knappable material lithotheque in the prehistory laboratory at the university of León, Spain. J Lithic Stud 5(2). https://doi.org/10.2218/jls.2926

Hubbard MJ, Waugh DA, Ortiz JD (2004) Provenance determination of chert by VIS/NIR diffuse reflectance spectrometry. Compass 78:119–129

Jain R, Sharma RU (2019) Airborne hyperspectral data for mineral mapping in Southeaster Rajasthan, Indica. Int J Appl Earth Obs Geoinf 81:137–145. https://doi.org/10.1016/j.jag.2019.05.007

Jain R, Bhu H, Purohit R (2022) Airborne imaging spectrometer dataset for spectral characterization and predictive mineral mapping using sub-pixel based classifier in parts of Udaipur. Rajasthan, India, Advances in Space Research,. https://doi.org/10.1016/j.asr.2022.08.032

Kassambara, A, Mundt, F (2020) factoextra: Extract and Visualize the Results of Multivariate Data Analyses. R package version 1.0.7.https://CRAN.R-project.org/package=factoextra. Accessed Sep 2023

Klein, C, Hurlbut Jr., CS (2008) Manual de Mineralogía. Reverté

Kokaly, R, Clark, R, Swayze, G, Livo, K, Hoefen, T, Pearson, N, … Klein, A (2017) USGS Spectral Library Version 7. U.S. Geological Survey Data Series 1035

Kruse F (2008) Expert system analysis of hyperspectral data. In: Proceedings of SPIE – The International Society for Optical Engineering, 6966, https://doi.org/10.1117/12.767554

Lackinger A (2014) Una aproximación experimental al empleo de la esteatita en la metalurgica prehistórica. In: González de la Fuente FJ, Paniagua Vara E, de Inés Sutíl P (Coord) Investigaciones arqueológicas en el Valle del Duero. Del Paleolítico a la Antigüedad Tardía: Actas de las III Jornadas de Jóvenes Investigadores del Valle del Duero, pp 343–357

Lantes-Suárez O, Prieto-Mártinez MP, Martínez Cortizas A (2009) Caracterización de la pasta blanca incrustada en decoraciones de campaniformes gallegos. Indagando sobre su procedencia. Proceedings of VIII Congreso Ibérico de Arqueometría, pp 87–100

Laukamp C (2011) Short wave infrared functional groups of rock-forming minerals. CSIRO. Report number EP115222. https://publications.csiro.au/publications/publication/PIcsiro:EP115222. Accessed Sep 2023

Lehnert LW, Meyer H, Obermeier WA, Silva B, Regeling B, Thies B, Bendix J (2019) Hyperspectral Data Analysis in R: The hsdar Package. J Stat Softw 89(12):1–23. https://doi.org/10.18637/jss.v089.i12

Liang H (2012) Advances in multispectral and hyperspectral imaging for archaeology and art conservation. Appl Phys A 106:309–323. https://doi.org/10.1007/s00339-011-6689-1

Liaw A, Wiener M (2002) Classification and Regression by randomForest. R News 2(3):18–22

Luengo J (1940) El castro de Morgovejo (León). Atlantis 15:170–177

Marín Suárez C (2011) De nómadas a castreños: El primer milenio antes de la Era en el sector centro-occidental de la Cordillera Cantábrica. Universidad Complutense, Tesis doctoral

Mutanga O, Skidmore AK (2004) Hyperspectral band depth analysis for a better estimation of grass biomass (Cenchrus ciliaris) measured under controlled laboratory conditions. Int J Appl Earth Obs Geoinf 5(2):87–96. https://doi.org/10.1016/j.jag.2004

Parish RM (2011) The application of visible/near-infrared reflectance (VNIR) spectroscopy to chert: A case study from the Dover Quarry sites, Tennessee. Geoarchaeology 26:420–439. https://doi.org/10.1002/gea.20354

Parish RM (2016) Reflectance spectroscopy as a chert sourcing method. Archaeologia Polona 54:115–128

Parish RM (2018) Lithic procurement patterning as a proxy for identifying Late Paleoindian group mobility along the Lower Tennessee River Valley. J Archaeol Sci Rep 22:313–323. https://doi.org/10.1016/j.jasrep.2016.03.028

Parish RM, Werra DH (2018) Characterizing "Chocolate" Flint Using Reflectance Spectroscopy. Archaeologia Polona 56:89–101. https://doi.org/10.23858/APa56.2018.007

Parish R (2013) The application of reflectance spectroscopy to chert provenance of mississippian symbolic weaponry. Dissertation, University of Memphis

Picollo M, Cucci C, Casini A, Stefani L (2020) Hyper-spectral imaging technique in the cultural heritage field: New possible scenarios. Sensors 20(10). https://doi.org/10.3390/s20102843

Pi-Puig T, Animas-Torices DY, Solé J (2020) Mineralogical and Geochemical Characterization of Talc from Two Mexican Ore Deposits (Oaxaca and Puebla) and Nine Talcs Marketed in Mexico: Evaluation of Its Cosmetic Uses. Minerals 10(5):380. https://doi.org/10.3390/min10050388

R Core Team (2021) R: A language and environment for statistical computing. R Foundation for Statistical Computing, Vienna, Austria. https://www.R-project.org/

Rincón Ramírez JA (2012) Modelización del registro y proceso de datos espectrales, referidos a superficies líticas, en un ámbito arqueológico.Dissertation, Universidad Politécnica de Madrid. https://doi.org/10.20868/UPM.thesis.15841

Romero Carnicero F, Górriz Gañán C (2007) Actividad textil y evidencias arqueológicas. In: Sanz Minguez C, Romero Carnicero F, Celis Sánchez J (Eds.) En los extremos de la región vaccea, Caja España, León, pp 115–118

Schmidt SC, Martini S, Staniuk R et al. (2022) Tutorial on classification in archaeology: Distance matrices, clustering methods and validation. Zenodo. Retrieved from https://doi.org/10.5281/zenodo.6325. Accessed Sep 2023

Siozos P, Philippidis A, Anglos D (2017) Portable laser-induced breakdown spectroscopy/diffuse reflectance hybrid spectrometer for analysis of inorganic pigments. Spectrochim Acta Part B at Spectrosc 137:93–100. https://doi.org/10.1016/j.sab.2017.09.005

Togari K (1979) Whiteness in colour of talc. Journal of the Faculty of Science, Hokkaido University. Series IV, Geology and mineralogy 19(1–2):213–220. https://eprints.lib.hokudai.ac.jp/dspace/bitstream/2115/36684/1/19_1-2_p213-220.pdf. Accessed Sep 2023

Van der Meer F (2004) Analysis of spectral absorption features in hyperspectral imagery. Int J Appl Earth Obs Geoinf 5(1):55–68. https://doi.org/10.1016/j.jag.2003.09.001

Vettori S, Benvenuti M, Camaiti M, Chiarantini L, Costagliola P, Moretti S, Pecchioni E (2008) Assessment of the deterioration status of historical buildings by hyperespectral imaging techniques. In: Proceedings of the Int. Conf. on In situ Monitoring of Monumental Surfaces, Firenze, pp 55–64

Villalobos García R (2016) Análisis de las transformaciones sociales en la Prehistoria Reciente de la Meseta Norte española (milenios vi-iii cal a.C.). Studia Archaeologica, 101. Edic. Univ. de Valladolid, Valladolid

Wisseman SU, Emerson TE, Hynes MR, Hughes RE (2004) Using a Portable Spectrometer to Source Archaeological Materials and to Detect Restorations in Museum Objects. J Am Inst Conserv 43:129–138. https://doi.org/10.1179/019713604806082519